Taylor & Francis
Taylor & Francis Group

Phase Transitions
A Multinational Journal

ISSN: 0141-1594 (Print) 1029-0338 (Online) Journal homepage: http://www.tandfonline.com/loi/gpht20

Magnetic behavior of a mixed spin-1 and spin-72 Blume–Capel model on the Bethe lattice in the presence of an applied magnetic field

M. Karimou, R. A. Yessoufou, F. K. Guedje, C. Aïnamon & F. Hontinfinde

To cite this article: M. Karimou, R. A. Yessoufou, F. K. Guedje, C. Aïnamon & F. Hontinfinde (2016): Magnetic behavior of a mixed spin-1 and spin-72 Blume–Capel model on the Bethe lattice in the presence of an applied magnetic field, Phase Transitions, DOI: 10.1080/01411594.2016.1179739

To link to this article: http://dx.doi.org/10.1080/01411594.2016.1179739

PHASE TRANSITIONS, 2016
http://dx.doi.org/10.1080/01411594.2016.1179739

Taylor & Francis
Taylor & Francis Group

Magnetic behavior of a mixed spin-1 and spin-$\frac{7}{2}$ Blume–Capel model on the Bethe lattice in the presence of an applied magnetic field

M. Karimou[a], R. A. Yessoufou[a,b], F. K. Guedje[a,b], C. Aïnamon[a,b] and F. Hontinfinde[a,b]

[a]Institute of Mathematics and Physical Sciences (IMSP), Dangbo, Republic of Benin; [b]Department of Physics, University of Abomey-Calavi, Abomey Calavi, Republic of Benin

ABSTRACT

The mixed spin-1 and spin-$\frac{7}{2}$ Blume–Capel model is investigated on the Bethe lattice in the presence of an external magnetic field h. The ground-state phase diagram which may be useful to explore interesting domains of the temperature phase diagrams of the model is constructed. The order parameters, the response functions, the internal energy and the free energy are thoroughly examined in order to characterize the nature of the phase transitions and to obtain the corresponding temperatures. Then, in the absence of the magnetic field, the temperature phase diagrams are displayed in the case of equal crystal field on the ($kT/|J|$, $D/|J|$) plane when $q = 3$, 4 and 6. The model exhibits first-order and second-order phase transitions and tricritical points where transition lines are connected. Besides these transitions, the system also shows compensation points for appropriate values of the model parameters.

ARTICLE HISTORY
Received 5 October 2015
Accepted 14 April 2016

KEYWORDS
Recursion relations; compensation phenomenon; stable states; magnetic field; multicritical points

PACS NUMBERS
05.50.+q; 05.70.Ce; 64.60.Cn; 75.10.Hk; 75.30.Gw

1. Introduction

In the last five decades, the Ising model has been one of the most largely used model to describe critical behaviors of several systems in nature. Recently, several extensions have been made in the spin-$\frac{1}{2}$ Ising model to describe a wide variety of systems. For example, the models consisting of mixed spins with different magnitudes are interesting extensions, forming the so-called mixed-spin Ising class. [1–5] Beyond that, magnetic materials have numerous and important technological applications: they find wide use in information storage devices, microwaves communication systems, electric power transformers and dynamo, and high-fidelity speakers.[6–9] Thus, in response to this increasing demand placed on the performance of magnetic solids, there has been a surge of interest in molecular-based magnetic materials.[10–13] Indeed, the discovery of the latter [14] has been one of the advances in modern magnetism. Many magnetic materials have two types of magnetic atoms regularly alternating which exhibit ferrimagnetism. In this context, a good description of their physical properties is given by means of mixed-spin configurations. The interest in studying magnetic properties of these materials is due to their reduced translational symmetry rather than to their single-spin counterparts, since they consist of two interpenetrating sublattices. Thus, ferrimagnetic materials are of great interest due to their possible technological applications and from a fundamental point of view. These materials are modeled by mixed-spin Ising models that can be built up by

CONTACT R. A. Yessoufou yesradca@yahoo.fr; yesradca@imsp-uac.org

infinite combinations of different spins, where the pairs constituted by spins with small values are the simplest: $\left(\frac{1}{2},1\right)$, $\left(\frac{1}{2},\frac{3}{2}\right)$, $\left(1,\frac{3}{2}\right)$, $\left(1,\frac{5}{2}\right)$, $\left(2,\frac{3}{2}\right)$, $\left(2,\frac{5}{2}\right)$ and so on.

There are many studies on mixed-spin Ising systems aiming to explain the physical properties of disordered systems. In this regard, there has been great interest in the study of magnetic properties of systems formed by two sublattices with different spins and crystal-field interactions.[15] Theoretically, such systems have been widely studied by a variety of methods, e.g. effective-field theory, [16−21] mean-field approximation,[22−26] renormalization group technique,[27,28] numerical simulations based on Monte Carlo (MC) [29−33] and exact recursion equations.[34−40] A more recent interest is to extend such investigations into a more general mixed-spin Ising model with one constituent spin-1 and the other constituent spin-$\frac{7}{2}$. In this context, Hadey [25] presented a mean-field theory based on the Bogoliubov inequality for Gibbs free energy study to elucidate only crystal field and magnetic field effects on the thermodynamic quantities, particularly on the existence and induction of compensation temperatures. Recently, Karimou et al.[39] studied the Blume−Capel version of the same model with two different single-ion anisotropies and found interesting results.

In the present work, we adopt the exact recursion equations technique to study the magnetic properties of the mixed spin-1 and spin-$\frac{7}{2}$ Ising model with equal crystal field on the Bethe lattice in the presence of a magnetic field. The purpose of this work is to analyze the influence of the crystal field and the magnetic field on the physical properties of the model.

The remainder of this work is arranged as follows. In Section 2, the formulation of the model on the Bethe lattice is specified and all the thermodynamical quantities of interest are calculated in terms of recursion relations. In the next section, a brief definition of the critical temperature of the model is given. Illustrations and discussions of numerical results are presented in Section 4. The last section is devoted to conclusion.

2. Description of the model on the Bethe lattice

The mixed-spin system on the Bethe lattice is shown in Figure 1. We consider the mixed spin-1 and spin-$\frac{7}{2}$ system consisting of two sublattices A and B. The sites of sublattice A are occupied by atoms of spins S_i, where $S_i = \pm 1, 0$. Those of the sublattice B are occupied by atoms of spins σ_j, where $\sigma_j = \pm\frac{7}{2}, \pm\frac{5}{2}, \pm\frac{3}{2}, \pm\frac{1}{2}$. In our case, the Bethe lattice is arranged such that the central spin is spin-1 and the next generation spin is spin-$\frac{7}{2}$ and so on to infinity. Thus the Ising Hamiltonian of

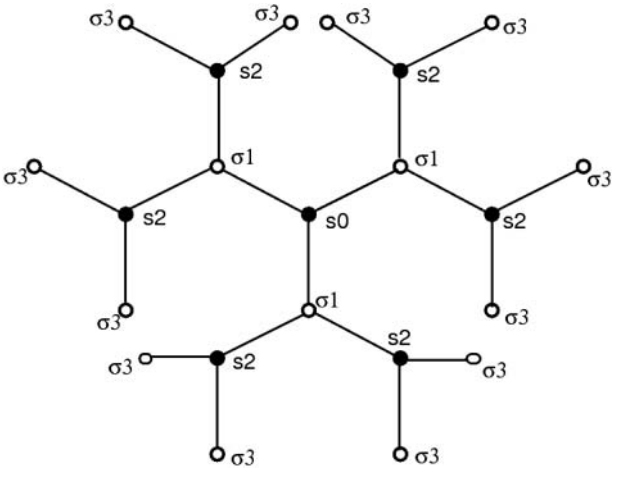

Figure 1. The mixed-spin Ising model consisting of two different magnetic atoms with spins values $s_i = 1$ and $\sigma_j = \frac{7}{2}$, respectively, defined on the Bethe lattice with coordination number $q = 3$.

such model on the Bethe lattice may be written as

$$H = -J \sum_{\langle i,j \rangle} \sigma_j S_i - D\left[\sum_i S_i^2 + \sum_j \sigma_j^2\right] - h\left[\sum_i S_i + \sum_j \sigma_j\right], \tag{1}$$

where $J < 0$ is the bilinear exchange coupling interaction strength. D and h are, respectively, the single-ion anisotropy (crystal field) and the longitudinal magnetic field acting on spins of the model.

In order to formulate the problem on the Bethe lattice, the partition function is the main ingredient which is given as

$$Z = \sum \exp\left[\beta\left(J \sum_{<i,j>} \sigma_j S_i + D(\sum_i S_i^2 + \sum_j \sigma_j^2) + h(\sum_i S_i + \sum_j \sigma_j)\right)\right]. \tag{2}$$

If the Bethe lattice is cut at the central spin S_0, it splits into q disconnected pieces. So, the partition function on the Bethe lattice can be written as

$$Z = \sum_{S_0} \exp\left[\beta(DS_0^2 + hS_0)\right] g_n^q(S_0), \tag{3}$$

where S_0 is the central spin value of the lattice, $g_n(S_0)$ is the partition function of an individual branch and the suffix n represents the fact that the sub-tree has n shells, i.e. n steps from the root to the boundary sites. If we continue to cut the Bethe lattice on sites σ_1 and S_2 which are, respectively, the nearest and next nearest of the central spin S_0, we can obtain the recurrence relations for $g_n(S_0)$ and $g_{n-1}(\sigma_1)$ as follows:

$$g_n(S_0) = \sum_{\{\sigma_1\}} \exp\left[\beta(JS_0\sigma_1 + D\sigma_1^2 + h\sigma_1)\right][g_{n-1}(\sigma_1))]^{q-1}, \tag{4}$$

$$g_{n-1}(\sigma_1) = \sum_{\{S_2\}} \exp\left[\beta(JS_2\sigma_1 + DS_2^2 + hS_2)\right][g_{n-2}(S_2))]^{q-1}. \tag{5}$$

Now we explicitly calculate some $g_n(S_0)$ and $g_{n-1}(\sigma_1)$ as follows:

$$\begin{aligned}
g_n(\pm 1) &= \sum_{\{\sigma_1\}} \exp\left[\beta(\pm J\sigma_1 + D\sigma_1^2 + h\sigma_1)\right][g_{n-1}(\sigma_1))]^{q-1} \\
&= e^{\beta\left(\pm\frac{7J}{2} + \frac{49}{4}D + \frac{7}{2}h\right)}\left[g_{n-1}\left(\frac{7}{2}\right)\right]^{q-1} + e^{\beta\left(\mp\frac{7J}{2} + \frac{49}{4}D - \frac{7}{2}h\right)}\left[g_{n-1}\left(\frac{-7}{2}\right)\right]^{q-1} \\
&\quad + e^{\beta\left(\pm\frac{5J}{2} + \frac{25}{4}D + \frac{5}{2}h\right)}\left[g_{n-1}\left(\frac{5}{2}\right)\right]^{q-1} + e^{\beta\left(\mp\frac{5J}{2} + \frac{25}{4}D - \frac{5}{2}h\right)}\left[g_{n-1}\left(\frac{-5}{2}\right)\right]^{q-1} \\
&\quad + e^{\beta\left(\pm\frac{3J}{2} + \frac{9}{4}D + \frac{3}{2}h\right)}\left[g_{n-1}\left(\frac{3}{2}\right)\right]^{q-1} + e^{\beta\left(\mp\frac{3J}{2} + \frac{9}{4}D - \frac{3}{2}h\right)}\left[g_{n-1}\left(\frac{-3}{2}\right)\right]^{q-1} \\
&\quad + e^{\beta\left(\pm\frac{J}{2} + \frac{1}{4}D + \frac{1}{2}h\right)}\left[g_{n-1}\left(\frac{1}{2}\right)\right]^{q-1} + e^{\beta\left(\mp\frac{J}{2} + \frac{1}{4}D - \frac{1}{2}h\right)}\left[g_{n-1}\left(\frac{-1}{2}\right)\right]^{q-1}
\end{aligned} \tag{6}$$

$$
\begin{aligned}
g_n(0) &= \sum_{\{\sigma_1\}} \exp\left[\beta(D\sigma_1^2 + h\sigma_1)\right][g_{n-1}(\sigma_1))]^{q-1} \\
&= e^{\beta\left(\frac{49}{4}D+\frac{7}{2}h\right)}\left[g_{n-1}\left(\frac{7}{2}\right)\right]^{q-1} + e^{\beta\left(\frac{49}{4}D-\frac{7}{2}h\right)}\left[g_{n-1}\left(\frac{-7}{2}\right)\right]^{q-1} \\
&\quad + e^{\beta\left(\frac{25}{4}D+\frac{5}{2}h\right)}\left[g_{n-1}\left(\frac{5}{2}\right)\right]^{q-1} + e^{\beta\left(\frac{25}{4}D-\frac{5}{2}h\right)}\left[g_{n-1}\left(\frac{-5}{2}\right)\right]^{q-1} \\
&\quad + e^{\beta\left(\frac{9}{4}D+\frac{3}{2}h\right)}\left[g_{n-1}\left(\frac{3}{2}\right)\right]^{q-1} + e^{\beta\left(\frac{9}{4}D-\frac{3}{2}h\right)}\left[g_{n-1}\left(\frac{-3}{2}\right)\right]^{q-1} \\
&\quad + e^{\beta\left(\frac{1}{4}D+\frac{1}{2}h\right)}\left[g_{n-1}\left(\frac{1}{2}\right)\right]^{q-1} + e^{\beta\left(\frac{1}{4}D-\frac{1}{2}h\right)}\left[g_{n-1}\left(\frac{-1}{2}\right)\right]^{q-1}
\end{aligned} \tag{7}
$$

$$
\begin{aligned}
g_{n-1}\left(\pm\frac{7}{2}\right) &= \sum_{\{S_2\}} \exp\left[\beta\left(\frac{\pm 7J}{2}S_2 + DS_2^2 + hS_2\right)\right][g_{n-2}(S_2))]^{q-1} \\
&= e^{\beta\left(\pm\frac{7J}{2}+D+h\right)}[g_{n-2}(1)]^{q-1} + e^{\beta\left(\mp\frac{7J}{2}+D-h\right)}[g_{n-2}(-1)]^{q-1} + g_{n-2}^{q-1}(0).
\end{aligned} \tag{8}
$$

$$
\begin{aligned}
g_{n-1}\left(\pm\frac{5}{2}\right) &= \sum_{\{S_2\}} \exp\left[\beta\left(\frac{\pm 5J}{2}S_2 + DS_2^2 + hS_2\right)\right][g_{n-2}(S_2))]^{q-1} \\
&= e^{\beta\left(\pm\frac{5J}{2}+D+h\right)}[g_{n-2}(1)]^{q-1} + e^{\beta\left(\mp\frac{5J}{2}+D-h\right)}[g_{n-2}(-1)]^{q-1} + g_{n-2}^{q-1}(0).
\end{aligned} \tag{9}
$$

$$
\begin{aligned}
g_{n-1}\left(\pm\frac{3}{2}\right) &= \sum_{\{S_2\}} \exp\left[\beta\left(\frac{\pm 3J}{2}S_2 + DS_2^2 + hS_2\right)\right][g_{n-2}(S_2))]^{q-1} \\
&= e^{\beta\left(\pm\frac{3J}{2}+D+h\right)}[g_{n-2}(1)]^{q-1} + e^{\beta\left(\mp\frac{3J}{2}+D-h\right)}[g_{n-2}(-1)]^{q-1} + g_{n-2}^{q-1}(0).
\end{aligned} \tag{10}
$$

$$
\begin{aligned}
g_{n-1}\left(\pm\frac{1}{2}\right) &= \sum_{\{S_2\}} \exp\left[\beta\left(\frac{\pm J}{2}S_2 + DS_2^2 + hS_2\right)\right][g_{n-2}(S_2))]^{q-1} \\
&= e^{\beta\left(\pm\frac{J}{2}+D+h\right)}[g_{n-2}(1)]^{q-1} + e^{\beta\left(\mp\frac{J}{2}+D-h\right)}[g_{n-2}(-1)]^{q-1} + g_{n-2}^{q-1}(0).
\end{aligned} \tag{11}
$$

After calculating all the $g_n(S_0)$ and $g_{n\ -\ 1}(\sigma_1)$, we can define the recursion relations for the spin-1 as

$$
Y_n = \frac{g_n(+1)}{g_n(0)}, \qquad Z_n = \frac{g_n(-1)}{g_n(0)}, \tag{12}
$$

and for the spin-$\frac{7}{2}$ as

$$\begin{aligned} A_{n-1} &= \frac{g_{n-1}\left(\frac{+7}{2}\right)}{g_{n-1}\left(\frac{-1}{2}\right)}, \qquad B_{n-1} = \frac{g_{n-1}\left(\frac{-7}{2}\right)}{g_{n-1}\left(\frac{-1}{2}\right)}, \\ C_{n-1} &= \frac{g_{n-1}\left(\frac{+5}{2}\right)}{g_{n-1}\left(\frac{-1}{2}\right)}, \qquad D_{n-1} = \frac{g_{n-1}\left(\frac{-5}{2}\right)}{g_{n-1}\left(\frac{-1}{2}\right)}, \\ E_{n-1} &= \frac{g_{n-1}\left(\frac{3}{2}\right)}{g_{n-1}\left(\frac{-1}{2}\right)}, \qquad F_{n-1} = \frac{g_{n-1}\left(\frac{-3}{2}\right)}{g_{n-1}\left(\frac{-1}{2}\right)} \\ G_{n-1} &= \frac{g_{n-1}\left(\frac{+1}{2}\right)}{g_{n-1}\left(\frac{-1}{2}\right)}. \end{aligned} \tag{13}$$

To investigate our model, we define two order parameters, the magnetization M and the corresponding quadrupolar moment Q. For the sublattice A, the order parameters are, respectively, defined by

$$M_{\mathrm{A}} = Z_{\mathrm{A}}^{-1} \sum\nolimits_{\{S_0\}} S_0 \exp\left[\beta(DS_0^2 + hS_0)\right] g_n^q(S_0), \tag{14}$$

$$Q_{\mathrm{A}} = Z_{\mathrm{A}}^{-1} \sum\nolimits_{\{S_0\}} S_0^2 \exp(\beta DS_0^2 + hS_0) g_n^q(S_0). \tag{15}$$

After some mathematical calculations, the two order parameters are explicitly given by

$$M_{\mathrm{A}} = \frac{e^{(\beta D)}\left(e^{(\beta h)} Y_n^q - e^{(-\beta h)} Z_n^q\right)}{e^{(\beta D)}\left(e^{(\beta h)} Y_n^q + e^{(-\beta h)} Z_n^q\right) + 1}, \tag{16}$$

$$Q_{\mathrm{A}} = \frac{e^{(\beta D)}\left(e^{(\beta h)} Y_n^q + e^{(-\beta h)} Z_n^q\right)}{e^{(\beta D)}\left(e^{(\beta h)} Y_n^q + e^{(-\beta h)} Z_n^q\right) + 1}. \tag{17}$$

In the same way, we also calculate the two order parameters for the sublattice B as follows:

$M_{\mathrm{B}} = \frac{M'_{\mathrm{B}}}{M^0_{\mathrm{B}}}$

$Q_{\mathrm{B}} = \frac{Q'_{\mathrm{B}}}{Q^0_{\mathrm{B}}}$.

where

$$\begin{aligned} M'_{\mathrm{B}} \;=\; & 7e^{\left(\frac{49}{4}\beta D\right)}\left(e^{\left(\frac{7}{2}\beta h\right)} A_{n-1}^q - e^{\left(\frac{-7}{2}\beta h\right)} B_{n-1}^q\right) \\ & + 5e^{\left(\frac{25}{4}\beta D\right)}\left(e^{\left(\frac{5}{2}\beta h\right)} C_{n-1}^q - e^{\left(\frac{-5}{2}\beta h\right)} D_{n-1}^q\right) \\ & + 3e^{\left(\frac{9}{4}\beta D\right)}\left(e^{\left(\frac{3}{2}\beta h\right)} E_{n-1}^q - e^{\left(\frac{-3}{2}\beta h\right)} F_{n-1}^q\right) \\ & + e^{\left(\frac{1}{4}\beta D\right)}\left(e^{\left(\frac{1}{2}\beta h\right)} G_{n-1}^q - e^{\left(\frac{-1}{2}\beta h\right)}\right) \end{aligned} \tag{18}$$

$$
\begin{aligned}
M_{\mathrm{B}}^{0} &= 2e^{\left(\frac{49}{4}\beta D\right)}\left(e^{\left(\frac{7}{2}\beta h\right)}A_{n-1}^{q}+e^{\left(\frac{-7}{2}\beta h\right)}B_{n-1}^{q}\right)\\
&\quad +2e^{\left(\frac{25}{4}\beta D\right)}\left(e^{\left(\frac{5}{2}\beta h\right)}C_{n-1}^{q}+e^{\left(\frac{-5}{2}\beta h\right)}D_{n-1}^{q}\right)\\
&\quad +2e^{\left(\frac{9}{4}\beta D\right)}\left(e^{\left(\frac{3}{2}\beta h\right)}E_{n-1}^{q}+e^{\left(\frac{-3}{2}\beta h\right)}F_{n-1}^{q}\right)\\
&\quad +2e^{\left(\frac{1}{4}\beta D\right)}\left(e^{\left(\frac{1}{2}\beta h\right)}G_{n-1}^{q}+e^{\left(\frac{-1}{2}\beta h\right)}\right)
\end{aligned}
\tag{19}
$$

$$
\begin{aligned}
Q_{\mathrm{B}}^{'} &= 49e^{\left(\frac{49}{4}\beta D\right)}\left(e^{\left(\frac{7}{2}\beta h\right)}A_{n-1}^{q}+e^{\left(\frac{-7}{2}\beta h\right)}B_{n-1}^{q}\right)\\
&\quad +25e^{\left(\frac{25}{4}\beta D\right)}\left(e^{\left(\frac{5}{2}\beta h\right)}C_{n-1}^{q}+e^{\left(\frac{-5}{2}\beta h\right)}D_{n-1}^{q}\right)\\
&\quad +9e^{\left(\frac{9}{4}\beta D\right)}\left(e^{\left(\frac{3}{2}\beta h\right)}E_{n-1}^{q}+e^{\left(\frac{-3}{2}\beta h\right)}F_{n-1}^{q}\right)\\
&\quad +e^{\left(\frac{1}{4}\beta D\right)}\left(e^{\left(\frac{1}{2}\beta h\right)}G_{n-1}^{q}+e^{\left(\frac{-1}{2}\beta h\right)}\right)
\end{aligned}
\tag{20}
$$

$$
\begin{aligned}
Q_{\mathrm{B}}^{0} &= 4e^{\left(\frac{49}{4}\beta D\right)}\left(e^{\left(\frac{7}{2}\beta h\right)}A_{n-1}^{q}+e^{\left(\frac{-7}{2}\beta h\right)}B_{n-1}^{q}\right)\\
&\quad +4e^{\left(\frac{25}{4}\beta D\right)}\left(e^{\left(\frac{5}{2}\beta h\right)}C_{n-1}^{q}+e^{\left(\frac{-5}{2}\beta h\right)}D_{n-1}^{q}\right)\\
&\quad +4e^{\left(\frac{9}{4}\beta D\right)}\left(e^{\left(\frac{3}{2}\beta h\right)}E_{n-1}^{q}+e^{\left(\frac{-3}{2}\beta h\right)}F_{n-1}^{q}\right)\\
&\quad +4e^{\left(\frac{1}{4}\beta D\right)}\left(e^{\left(\frac{1}{2}\beta h\right)}G_{n-1}^{q}+e^{\left(\frac{-1}{2}\beta h\right)}\right).
\end{aligned}
\tag{21}
$$

In order to determine the compensation temperature, one has to define the global magnetization M_{net} of the model which is given by

$$M_{\mathrm{net}}=\frac{M_{\mathrm{A}}+M_{\mathrm{B}}}{2}. \tag{22}$$

To really study the model in detail and single out the influence of the applied magnetic field on the magnetic properties of the model, we have also examined the thermal variations of the response functions, i.e the susceptibilities, the specific heat and the internal energy defined, respectively, by

$$
\begin{aligned}
\chi_{\mathrm{Total}} &= \chi_{\mathrm{A}}+\chi_{\mathrm{B}}\\
&= \left(\frac{\partial M_{\mathrm{A}}}{\partial h}\right)_{h=0}+\left(\frac{\partial M_{\mathrm{A}}}{\partial h}\right)_{h=0}
\end{aligned}
\tag{23}
$$

$$C=-\beta^{2}\frac{\partial^{2}(-\beta F')}{\partial\beta^{2}} \tag{24}$$

$$\frac{U}{N|J|}=-k_{\mathrm{B}}T^{2}\frac{\partial}{\partial T}\left(\frac{F'}{k_{\mathrm{B}}T}\right), \tag{25}$$

where F' is the free energy.

So, using the definition of the free energy $F' = -kT\ln(Z)$ in the thermodynamic limit $(n \to \infty)$ and in order to introduce the recursion relations, we can rewrite the free energy as

$$F'/J = -\frac{1}{\beta'}\left[\frac{q-1}{2-q}\ln F_1 + \frac{1}{2-q}\ln F_2 + \ln F_3\right], \tag{26}$$

where $\beta' = \beta J$, $F_1 = \frac{g_{n-1}(-1/2)}{g_n^{q-1}(0)}$, $F_2 = \frac{g_n(0)}{g_{n-1}^{q-1}(-1/2)}$ and $F_3 = \frac{Z}{g_0^q(0)}$.

After some mathematical manipulations, the free energy expression in terms of recursion relations is explicitly given by

$$\begin{aligned}
F'/J = & -\frac{1}{\beta'}\left\{\frac{q-1}{2-q}\ln\left[e^{\beta\left(\frac{-J}{2}+D+h\right)}Y_n^{q-1} + e^{\beta\left(\frac{J}{2}+D-h\right)}Z_n^{q-1} + 1\right]\right\} \\
& -\frac{1}{\beta'}\left\{\ln\left[e^{\beta(D+h)}Y_n^q + e^{\beta(D-h)}Z_n^q + 1\right]\right\} \\
& -\frac{1}{\beta'}\left\{\frac{1}{2-q}\ln\left[e^{\beta\left(\frac{49D}{4}+\frac{7h}{2}\right)}A_{n-1}^{q-1} + e^{\beta\left(\frac{49D}{4}-\frac{7h}{2}\right)}B_{n-1}^{q-1}\right.\right. \\
& +e^{\beta\left(\frac{25D}{4}+\frac{5h}{2}\right)}C_{n-1}^{q-1} + e^{\beta\left(\frac{25D}{4}-\frac{5h}{2}\right)}D_{n-1}^{q-1} \\
& +e^{\beta\left(\frac{9D}{4}+\frac{3h}{2}\right)}E_{n-1}^{q-1} + e^{\beta\left(\frac{9D}{4}-\frac{3h}{2}\right)}F_{n-1}^{q-1} \\
& \left.\left.+e^{\beta\left(\frac{D}{4}+\frac{h}{2}\right)}G_{n-1}^{q-1} + e^{\beta\left(\frac{D}{4}-\frac{h}{2}\right)}\right]\right\}.
\end{aligned} \tag{27}$$

3. Definition of the critical temperatures

The Curie temperature or second-order transition temperature T_c is the temperature at which both sublattice magnetizations and the global magnetization go to zero continuously. T_c separates the ordered ferrimagnetic phase (F) from the disordered paramagnetic phase (P). At T_c, one can obtain explicit expressions of the recursion relations as follows:

For the spin-1,

$$Y_n = Z_n = \frac{Y_1}{Y_0}, \tag{28}$$

where

$$\begin{aligned}
Y_1 \quad = \quad & e^{\frac{49\beta D}{4}}\cosh\left(\frac{7\beta J}{2}\right)A_{n-1}^{q-1} + e^{\frac{25\beta D}{4}}\cosh\left(\frac{5\beta J}{2}\right)C_{n-1}^{q-1} \\
& +e^{\frac{9\beta D}{4}}\cosh\left(\frac{3\beta J}{2}\right)E_{n-1}^{q-1} + e^{\frac{\beta D}{4}}\cosh\left(\frac{\beta J}{2}\right)G_{n-1}^{q-1}
\end{aligned}$$

$$Y_0 = 2\left(e^{\frac{49\beta D}{4}}A_{n-1}^{q-1} + e^{\frac{25\beta D}{4}}C_{n-1}^{q-1} + e^{\frac{9\beta D}{4}}E_{n-1}^{q-1} + e^{\frac{\beta D}{4}}G_{n-1}^{q-1}\right),$$

and for the spin-$\frac{7}{2}$,

$$A_{n-1} = B_{n-1} = \frac{e^{\beta D}\cosh\left(\frac{7\beta J}{2}\right) Y_n^{q-1} + 1}{e^{\beta D}\cosh\left(\frac{\beta J}{2}\right) Y_n^{q-1} + 1} \tag{29}$$

$$C_{n-1} = D_{n-1} = \frac{e^{\beta D}\cosh\left(\frac{5\beta J}{2}\right) Y_n^{q-1} + 1}{e^{\beta D}\cosh\left(\frac{\beta J}{2}\right) Y_n^{q-1} + 1} \tag{30}$$

$$E_{n-1} = F_{n-1} = \frac{e^{\beta D}\cosh\left(\frac{3\beta J}{2}\right) Y_n^{q-1} + 1}{e^{\beta D}\cosh\left(\frac{\beta J}{2}\right) Y_n^{q-1} + 1}. \tag{31}$$

In addition to the thermal variations of the order parameters and the global magnetization of the model, we also analyze the free energy F' of the model in order to identify the first-order transition temperature T_t.

We also investigate the compensation temperature T_{comp} at which the global magnetization goes to zero while both sublattice magnetizations cancel each other. T_{comp} is found by locating the crossing point between the absolute values of sublattice magnetizations, i.e.

$$|M_A(T_{comp})| = |M_B(T_{comp})| \neq 0. \tag{32}$$

Thus, we are now ready to study the thermal variations of the calculated thermodynamical quantities of interest and to construct the finite-temperature phase diagrams of the model for $q = 3$, 4 and 6.

4. Numerical results and discussions

In this section, we present and discuss the results we obtained for the thermal behavior of the order parameters, the response functions, the internal energy, the free energy and the finite-temperature phase diagrams of the model. For this, we start discussions of the ground-state phase diagram which is very useful for the understanding of the obtained finite-temperature phase diagrams.

4.1. Ground-state phase diagram

Before proceeding to the discussions of the numerical results for the temperature dependence of the magnetic properties of the model, we first investigate the ground-state phase diagram. The ground-state structure of the model can be found by comparing the values of the energy H_0 for different spin configurations. H_0 may be written as

$$H_0 = S\sigma - \frac{1}{q|J|}\left[D(S^2 + \sigma^2) + h(S + \sigma)\right]. \tag{33}$$

Because of the ferrimagnetic coupling J and positive field ($h \geq 0$), we only find eight possible pairs of spins. Computational analysis of the corresponding energies in the $(\frac{D}{q|J|}, \frac{h}{q|J|})$ plane yields the ground-state phase diagram displayed in Figure 2. The investigated mixed-spin Ising model has the usual symmetry. So, all ground states for negative field ($h < 0$) can be obtained from the corresponding ones at positive field, simply by reversing all spin orientations. The energies and the conditions for the occurrence of the eight possible states are shown in Table 1. This diagram shows some key features, in particular, the existence of seven multicritical points (A_1, A_2, $\cdots$, A_7) and coexistence lines where the spin pair energy of some phases coincides. In the absence of the magnetic field, for a given value of q and $D/q|J| \geq -\frac{1}{2}$, five saturation values exist for M_B whereas for M_A, ∓ 1 is the only one saturation value. Thus, we get the thermodynamic phases $\left(\mp 1, \pm\frac{7}{2}\right)$, $\left(\mp 1, \pm\frac{5}{2}\right)$ and $\left(\mp 1, \pm\frac{3}{2}\right)$, and at the borders of

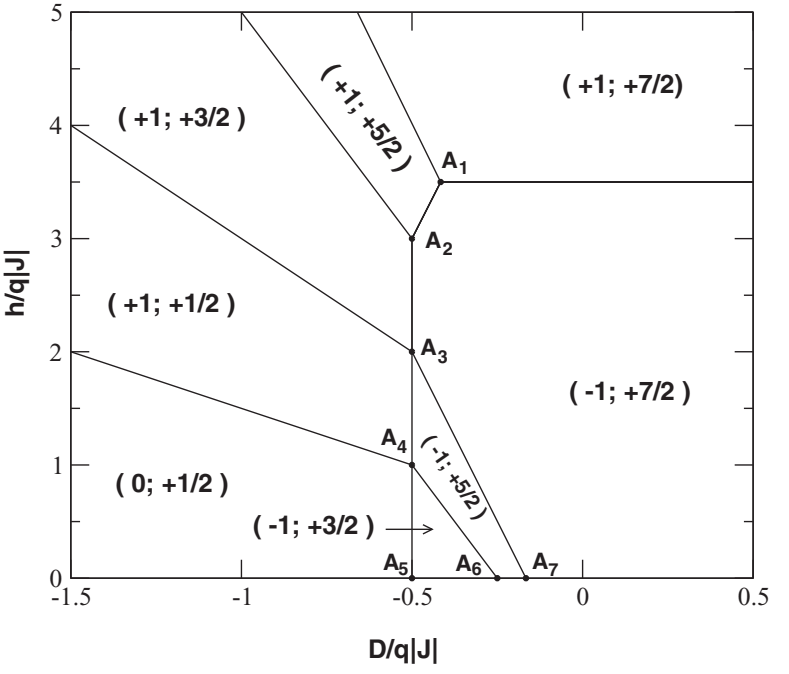

Figure 2. Ground-state phase diagram of the mixed spin-1 and spin-7/2 Ising ferrimagnetic model with equal crystal field D for the two sublattices in the $(\frac{h}{q|J|}, \frac{D}{q|J|})$ plane. Eight stable phases exist. Along the $\frac{D}{q|J|}$-axis and for $\frac{D}{q|J|} \geq -\frac{1}{2}$, two hybrid phases may prevail at the multicritical points A_6 and A_7 (see text).

these phases, two hybrid phases, $(\mp 1, \pm 3)$ and $(\mp 1, \pm 2)$ at the multicritical points A_7 and A_6, respectively. These hybrid phases should correspond to cases where the sublattice B is half−half covered by spins of the two neighboring phases. It is important to indicate that the ground-state phase diagram is very useful because it helps to check the reliability of the theoretical results and to classify different phase regions of the model for the phase diagrams at nonzero temperature.

4.2. Thermal variations of the order parameters, the response functions and the internal energy

As it is explained above, the thermal variations of the order parameters, the response functions, the internal energy and free energy for the present model were obtained in terms of recursion relations.

Table 1. Energies and conditions for the occurrence of the eight spin configurations in the ground-state phase diagram for mixed spin-1 and spin-$\frac{7}{2}$ ferrimagnetic Ising model under the magnetic field h ($h > 0$).

Spin configuration	Ground-state energy per site (H_0) of the state	Conditions for occurrence
$(+1, +\frac{7}{2})$ I	$-\frac{7qJ}{2} - \frac{53D}{4} - \frac{9h}{2}$	$-7qJ - 2h > 0$ and $-qJ - 6D - h < 0$
$(+1, -\frac{7}{2})$ II	$\frac{7qJ}{2} - \frac{53D}{4} - \frac{5h}{2}$	$h > 0$, $-7qJ - 2h < 0$, $6qJ - 6D + h < 0$, $2D + 1 > 0$ and $-qJ - 6D - h < 0$
$(+1, +\frac{5}{2})$ III	$-\frac{5qJ}{2} - \frac{29D}{4} - \frac{7h}{2}$	$6qJ - 6D + h > 0$, $-qJ - 6D - h > 0$, and $-qJ - 4D - h < 0$
$(+1, -\frac{5}{2})$ IV	$\frac{5qJ}{2} - \frac{29D}{4} - \frac{3h}{2}$	$h > 0$, $qJ - 6D - h > 0$, $2D + 1 > 0$ and $qJ - 4D - h < 0$
$(+1, +\frac{3}{2})$ V	$-\frac{3qJ}{2} - \frac{13D}{4} - \frac{5h}{2}$	$-qJ - 2D - h > 0$, $2D + 1 < 0$ and $-qJ - 4D - h > 0$
$(+1, -\frac{3}{2})$ VI	$\frac{3qJ}{2} - \frac{13D}{4} - \frac{h}{2}$	$h > 0$, $qJ - 4D - h > 0$ and $2D + 1 > 0$
$(+1, +\frac{1}{2})$ VII	$-\frac{qJ}{2} - \frac{5D}{4} - \frac{3h}{2}$	$h > 0$, $-qJ - 2D - h < 0$, $2D + 1 < 0$ and $-\frac{qJ}{2} - D - h > 0$
$(0, +\frac{1}{2})$ VIII	$-\frac{D}{4} - \frac{h}{2}$	$h > 0$, $-\frac{qJ}{2} - D - h < 0$ and $2D + 1 < 0$

The thermal behaviors of the order parameters play a crucial role in obtaining the finite-temperature phase diagrams of the system: when the magnetization curves go to zero continuously separating the ferrimagnetic phase from the paramagnetic phase, one gets the second-order phase transition or Curie temperature, i.e. the temperature at which magnetizations vanish. In the case of jumps in the magnetization curves followed by a discontinuity of the first derivative of the free energy F', one gets a first-order transition temperature. Besides these two temperatures, there is another temperature called compensation temperature defined as the temperature where the global magnetization becomes zero before the critical temperature. Therefore, in order to identify transition and compensation lines, one has to study the thermal behaviors of the considered thermodynamical quantities of the model. Now, we can present some results concerning the thermal behaviors of the order parameters, the response functions and the internal energy in the absence of the magnetic field h when $q = 3$, 4 and 6.

Figure 3 illustrates some thermal variations of the sublattice magnetizations M_1 and $M_{\frac{7}{2}}$ when $q = 3$, 4 and 6 for selected values of the crystal field $\frac{D}{|J|}$. From panels (a) to (b), we have depicted the thermal behaviors of sublattice magnetizations M_1 and $M_{\frac{7}{2}}$ as functions of the temperature for selected values of $D/|J|$ when $q = 3$, 4. The results are in perfect agreement with the ground-state phase diagram concerning the saturation values. Indeed, M_1 falls from its unique saturation value ∓ 1 with the increasing temperature whereas $M_{\frac{7}{2}}$ shows five saturation values. The behaviors of the sublattice magnetizations M_1 and $M_{\frac{7}{2}}$ are quite similar. Also, one can notice that all the curves are continuous and the Curie temperature T_c at which both magnetization curves go to zero increases with the crystal field $D/|J|$ and the coordination number q. In the last panel, we have displayed the temperature variations of the sublattice magnetizations for the selected values of the crystal field when $q = 6$. One notices that the model also exhibits first-order transition indicated here by T_t. Especially, from this panel one remarks that the model presents three different first-order transition temperatures, namely T_{t_1}, T_{t_2} and T_{t_3}.

In Figure 4, we have displayed the thermal behaviors of the sublattice magnetizations and corresponding susceptibilities when $q = 3$, 4 and $D/|J| = 1$. From this figure, one can notice that the model only exhibits the second-order phase transition and the transition temperature T_c at which the transition occurs, increases with the increasing coordination number q. Here, T_c separates the ferrimagnetic phase $\left(\mp 1, \pm \frac{7}{2}\right)$ from the paramagnetic phase (P) and $T_c/|J| = 5.061$ (respectively, $T_c/|J| = 7.364$) for $q = 3$ (respectively for $q = 4$). Also, one remarks that for $T \to T_c$, $\chi_1 \to +\infty$ whereas $\chi_{7/2} \to -\infty$. For $T > T_c$, the susceptibility χ_1 rapidly decreases whereas the susceptibility $\chi_{7/2}$ rapidly increases when the temperature increases and very far from the Curie temperature T_c, $\chi_1 \to 0$ and $\chi_{7/2} \to 0$.

On the other hand, to really confirm that the model only exhibits the second-order transition for $q = 3$, 4, we have plotted in Figure 5 the temperature dependence variations of the specific heat and the internal energy for various values of the crystal field as indicated in the figure. Both the specific heat and the internal energy rapidly increase with the increasing temperature and make peak without jump discontinuities at the same T_c. By increasing the strength of the crystal field and the coordination number, the T_c, at which the transition occurs, increases and this is easily observed by comparing results from different panels of Figure 5. The results obtained in this figure also confirm that the system only presents second-order transition for the coordination numbers 3 and 4.

In order to prove that the model really shows three first-order transition temperatures as shown in the last panel of Figure 3 for $q = 6$, we have illustrated in Figure 6, the temperature dependence of sublattice magnetizations, the specific heat and the free energy for the same values of the system parameters as it is considered in the last panel of Figure 3. The sublattice magnetizations, the specific heat and also the free energy F' simultaneously exhibit three different jump discontinuities at three different first-order temperatures indicated respectively by $T_{t_1/|J|} = 0.116$, $T_{t_2/|J|} = 0.446$ and $T_{t_3/|J|} = 0.832$. From this figure, one can confirm the existence of three different first-order transition temperatures.

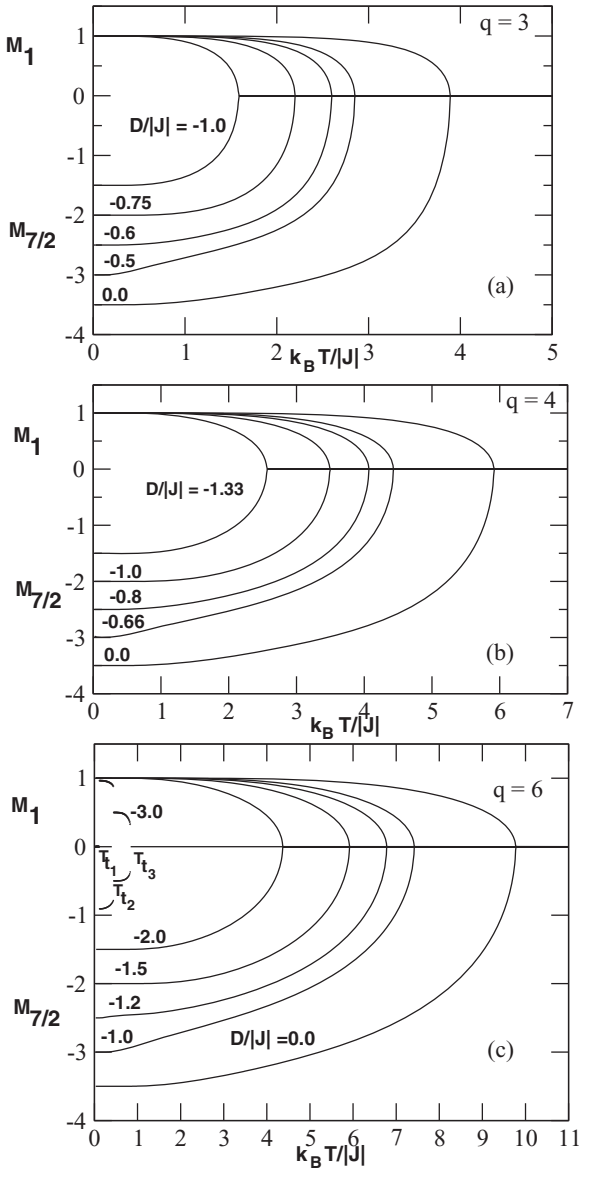

Figure 3. Sublattice magnetizations of the model as functions of the reduced temperature $kT/|J|$ when $q = 3$, 4 and 6 for various values of the crystal field interactions D. Panel (a): Curves are displayed for $q = 3$ and selected values of $D/|J|$ indicated on the curves. Panel (b): Curves are displayed for $q = 4$ and selected values of $D/|J|$ indicated on the curves. Panel (c): Curves are displayed for $q = 6$ and selected values of $D/|J|$ indicated on the curves. For $q = 3$, 4, the model shows only second-order transition, but for $q = 6$, the model exhibits second-order and first-order transitions. T_c and T_t are, respectively, the second-order and first-order temperatures.

Let us now discuss the thermal variations of the sublattice magnetizations, the corresponding response functions and the internal energy of the system in the presence of the longitudinal magnetic field h.

Figure 7 expresses the effects of an applied magnetic field h on the magnetic properties of the model when $q = 3$ and $D/|J| = 0.15$ for selected values of $h/|J|$. From panel (a) to panel (b), the sublattice magnetizations continuously decrease from their saturation values to nonzero values when the temperature increases. The remaining values of the sublattice magnetizations are more

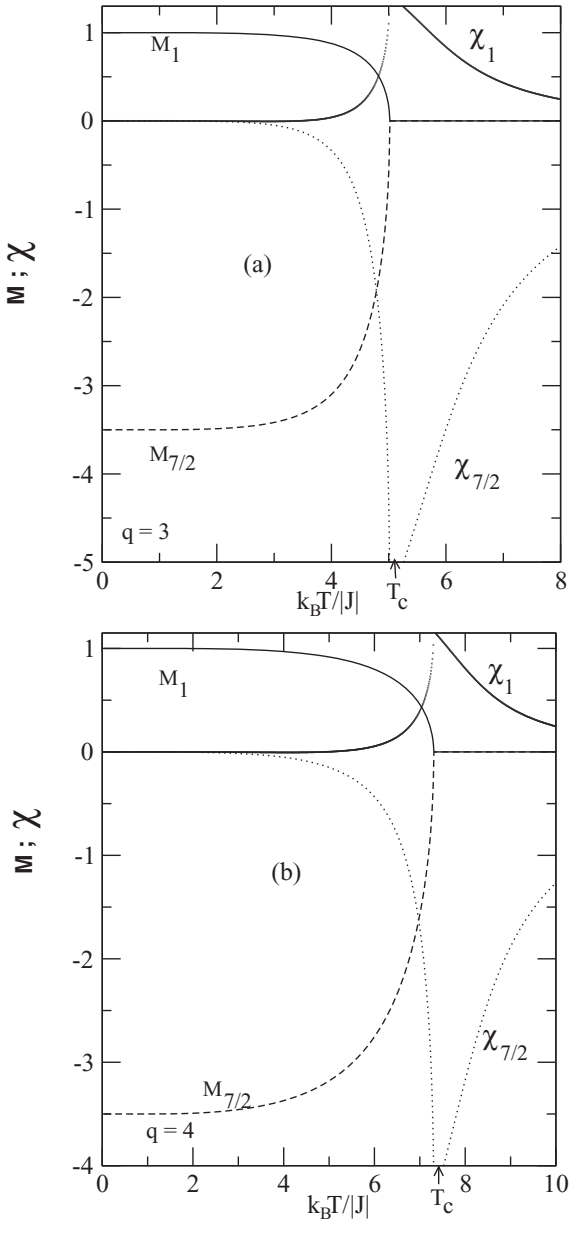

Figure 4. Thermal variations of sublattice magnetizations and corresponding susceptibilities are calculated for $q = 3$, 4, and the reduced crystal field $D/|J| = 1$ as shown in the figure from panel (a) to panel (b). Values of the physical parameters considered for the system are indicated in different panels.

important when the value of the applied magnetic field increases. So, one can observe that the system does not present any transition when $h/|J| \neq 0$. It is important to indicate that in the case of $h/|J| = 0$, the model exhibits the second-order transition at a Curie temperature $T_c/|J| = 4.153$, where the two sublattice magnetizations continuously go to zero after decreasing from their saturation values at $T = 0$. In panels (c)−(e), we have displayed the temperature dependence of the total susceptibility χ_T, the specific heat C and the internal energy U. One can see from these panels that the response functions and the internal energy indicate a second-order transition which occurs at the same $T_c/|J|$ as in the case of $h/|J| = 0$. For $h/|J| \neq 0$ and $T > T_c$, the response functions exhibit a

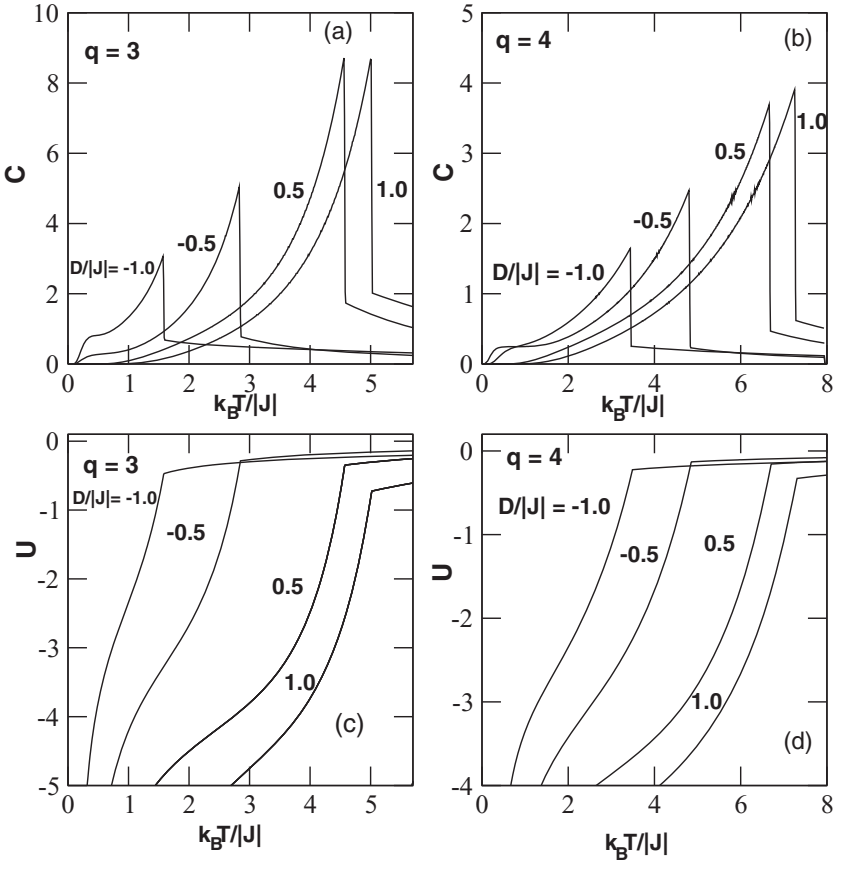

Figure 5. Thermal variations of the specific heat and internal energy are calculated for $q = 3, 4$, and selected values of the crystal field $D/|J|$ as shown in the figures from panel (a) to panel (d). Values of the physical parameters considered for the system are indicated in different panels. Analysis of the different panels of this figure shows that the model only exhibits second-order transition for $q = 3, 4$.

maximum and the height of the maximum decreases when the value of the applied magnetic field increases.

To show the influence of $D/|J|$ on the system properties, we have illustrated in Figure 8, the thermal variations of the response functions for some values of the system parameters: $h/|J| = 0.5$; $q = 3, 4$ and varying $D/|J|$. Considering the different panels of Figure 8, one observes that the response functions show interesting behaviors. Indeed, the two studied response functions globally show a maximum at a certain value of the temperature. This temperature increases with the coordination number and the strength of the crystal field. It is important to mention that the height of the maximum of the two response functions also increases by increasing the strength of the crystal field.

4.3. Finite-temperature phase diagrams

After all the above calculations, we can illustrate the finite-temperature phase diagrams of the model. So, in Figure 9, we have constructed the phase diagrams of the system in the $(D/|J|, kT/|J|)$ plane in the absence of the magnetic field when $q = 3, 4$ and 6. In the different phase diagrams, the solid, the dashed, the dotted lines and the filled circles indicate, respectively, second-order transition, first-order transition, compensation lines and tricritical points. The two filled triangles indicate the two multicritical points A_6 and A_7 found in the ground-state phase diagram displayed in Figure 2.

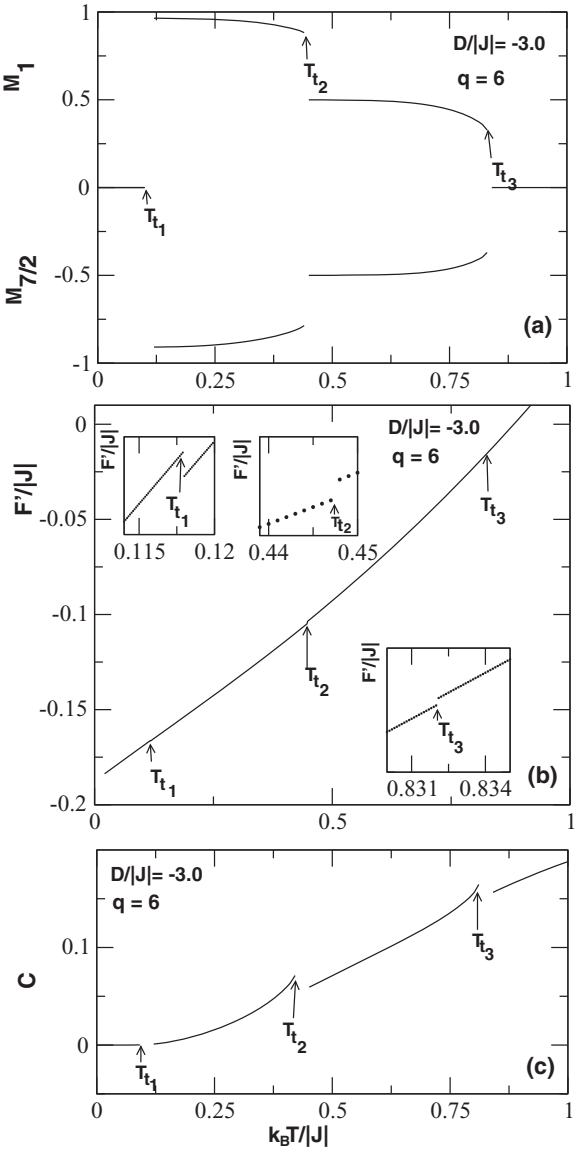

Figure 6. Temperature dependence of sublattice magnetizations, the specific heat and the free energy when $D/|J| = -3$ and $q = 6$. From different panels, one can conclude that the model exhibits first-order transition at three different temperatures where the different thermodynamical quantities studied here present three different jump discontinuities.

From this figure, some interesting properties of the system are singled out. Indeed, for all values of the coordination number q, the compensation lines are unclosed loops which are obtained by the collection of the compensation temperatures. From panel (a) to panel (b) where $q = 3$ and 4, the transition lines are only of the second order, separate the ferrimagnetic phase (F) from the paramagnetic phase (P) and go to the zero temperature at $D/|J| = -\frac{q}{2}$. Also, one can observe that (1) when $D/|J| > -\frac{q}{6}$, the second-order phase transition turns from ferrimagnetic phase **II** to the disordered paramagnetic phase P. (2) For $-\frac{q}{4} < D/|J| < -\frac{q}{6}$, the second-order phase transition is from the ferrimagnetic **IV** to the paramagnetic phase P. (3) When $-\frac{q}{2} < D/|J| < -\frac{q}{4}$, the second-order phase transition is from the ferrimagnetic phase **VI** to the paramagnetic phase P. (4) For $D/|J| = -\frac{q}{6}$,

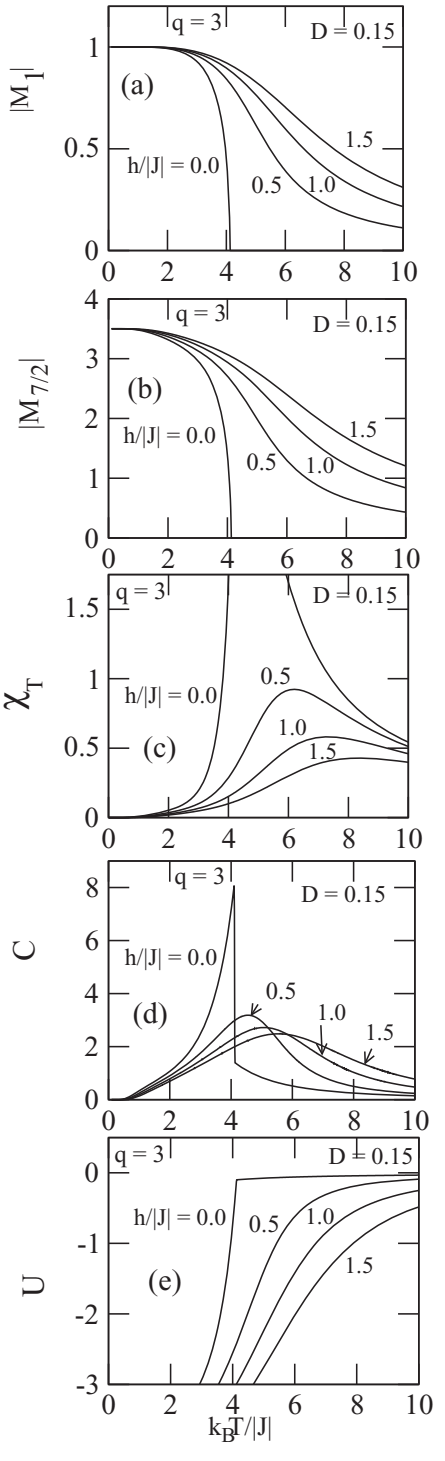

Figure 7. Thermal variations of sublattice magnetizations, the corresponding response functions and the internal energy of the model when $D/|J| = 0.15$ for selected values of the magnetic field $h/|J|$ as shown in different panels. From the analysis of different panels, one can remark that the model only presents phase transition when $h/|J| = 0$. For $h/|J| \neq 0$, the remaining magnetizations become more important when the value of the magnetic field increases.

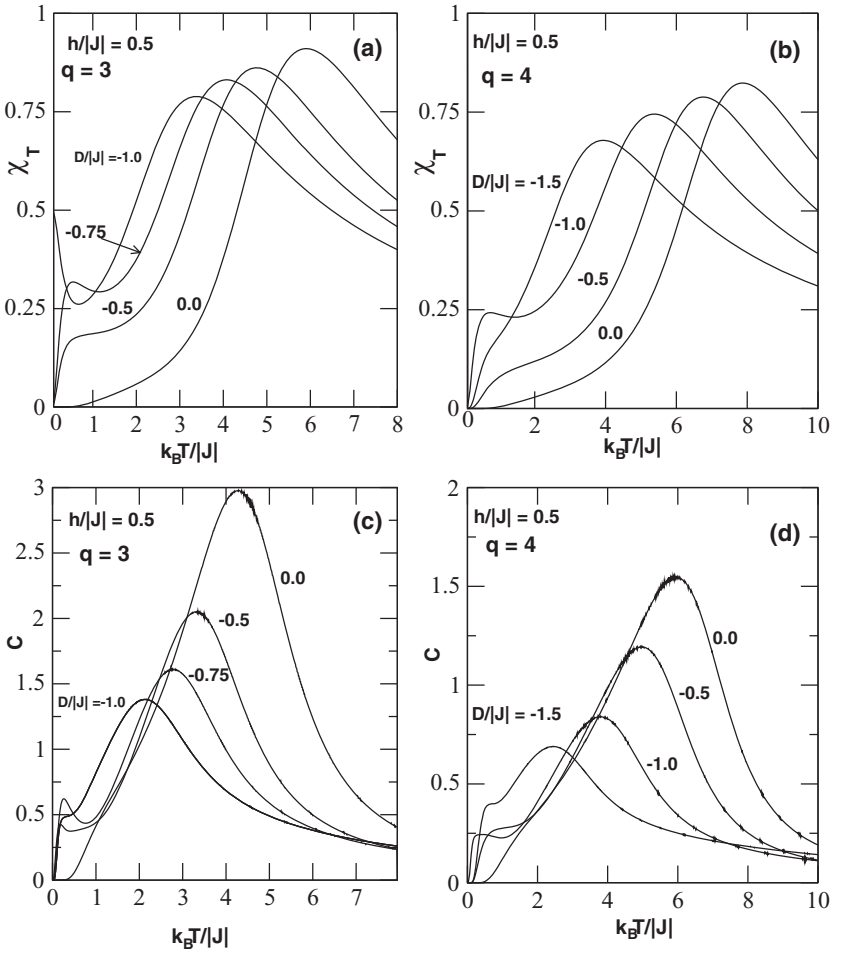

Figure 8. Temperature variations of the response functions of the model at selected values of $D/|J|$ indicated in different curves illustrated for $q = 3$, 4 and $h/|J| = 0.5$.

respectively, $D/|J| = -\frac{q}{4}$, the second-order transition phase is from the hybrid phase (∓ 1, ± 3), respectively, the hybrid phase (∓ 1, ± 2) to the paramagnetic phase P.

In the last panel where the phase diagram is constructed for $q = 6$, the model shows a tricritical point located by ($D_{\text{tri}}/|J| \simeq -2.99$, $kT_{\text{tri}}/|J| \simeq 0.832$) where the second-order transition line is connected to the first-order transition line, and the first-order transition line existing at very low temperatures goes also to zero temperature at $D/|J| = -\frac{q}{2}$. Here, also one can notice similar results concerning the transition from the different ferrimagnetic phases to the paramagnetic phase P as in the case of $q = 3$ and 4. But for $-\frac{q}{2} < D/|J| < D_{\text{tri}}/|J|$, the transition is of the first order and is from the ferrimagnetic phase **VI** to the paramagnetic phase P. It is important to indicate that the Curie temperature at which the second-order transition occurs increases with the strength of the crystal field D and the coordination number q.

In order to check that reliable compensation temperatures are found, we have examined the thermal variations of the global magnetization M_{net} of the system as a function of the temperature for $q = 4$ and $D/|J| = -1.992$ as shown in panel (a) of Figure 10. The global magnetization vanishes twice before going to the Curie temperature T_{c}. Here, the two compensation temperatures are, respectively, $T_{\text{comp1}}/|J| = 0.069$ and $T_{\text{comp2}}/|J| = 0.536$. This indicates that the model globally shows two compensation temperatures. Our results concerning the existence of the compensation

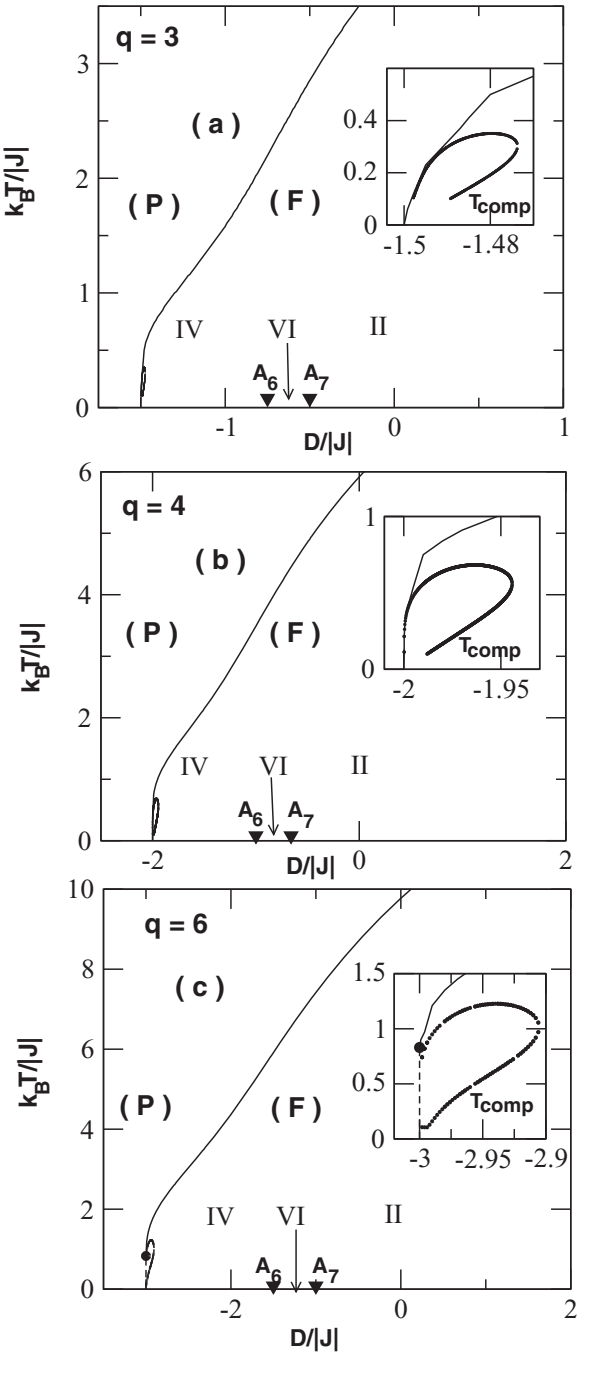

Figure 9. Finite-temperature phase diagrams of the model in the ($D/|J|$, $kT/|J|$) plane. The solid, dashed, dotted lines and filled circles indicate, respectively, second-order transition line, first-order transition line, compensation line and tricritical points. Panel (a): $q = 3$; panel (b): $q = 4$; panel (c): $q = 6$. Here, the model presents tricritical behavior in the case of $q = 6$ and the compensation lines are unclosed loops for all values of q. The multicritical points A_6 and A_7, which, respectively, indicate the positions of the hybrid phases ($\mp 1, \pm 2$) and ($\mp 1, \pm 3$), and separate the ferrimagnetic phases VI, IV and II.

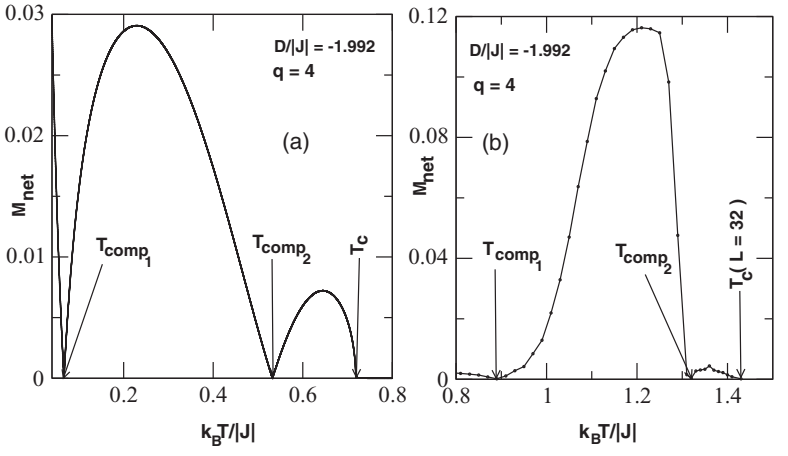

Figure 10. Thermal behavior of the global magnetization of the model are examined by means of two methods. Panel (a): Bethe approach method; panel (b): Monte Carlo (MC) simulations method. The two methods are qualitatively in perfect agreement concerning the existence of the compensation points of the model.

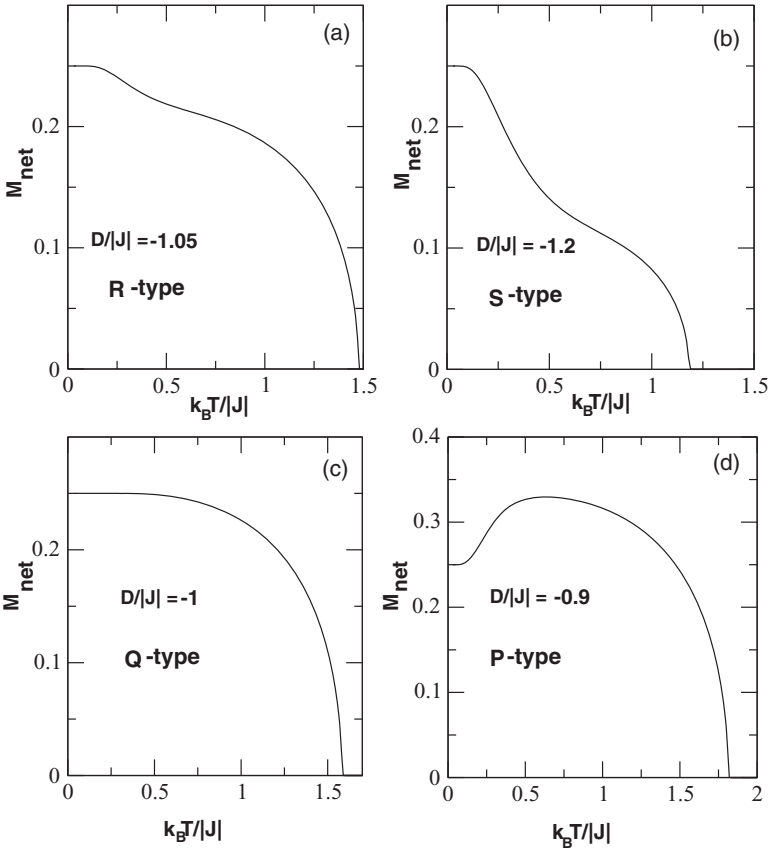

Figure 11. M_{net} as a function of the temperature for selected values of the crystal field when $q = 3$ as indicated in different panels. The model shows the R-, S-, Q- and P-type of compensation behaviors as classified in the extended Néel nomenclature.

temperatures are in perfect agreement with [25], where the same model is investigated. Also, to get reliable insight on the calculated compensation temperatures in panel (a), we have used the standard MC simulations with the usual Metropolis algorithm [41] on a relatively small system of 32×32 lattice size with periodic boundary conditions. The previous results have been checked for $q = 4$ and $D/|J| = -1.992$. A number of 5×10^5 MC steps and six independent runs are performed for statistical averages. Physical quantities of interest are calculated after the system reaches a thermal equilibrium at the considered temperature. As indicated in panel (b), two compensation temperatures are also recovered. It emerges that the MC simulations are in qualitative agreement with results found by the Bethe lattice approach. Extensive simulations and larger system sizes are certainly needed to get more accurate quantitative results. Since the Bethe lattice approach neglects spin correlations that are importantly close to the Curie temperature, one may not expect to get quantitative agreement with results displayed in panel (a).

Also, we investigated the global magnetization as a function of the temperature and obtained some compensation types of Ising model. Figure 11 shows temperature dependencies of the global magnetization M_{net} for selected values of the crystal field when $q = 3$. As seen from Figure 11, the model exhibits four types of compensation behaviors, namely R-, S-, Q- and P-type compensation behaviors as classified in the extended Néel nomenclature.[42]

5. Conclusion

In this paper, we report results on the molecular magnetism of the mixed spin-1 and spin-$\frac{7}{2}$ Blume−Capel ferrimagnetic model on the Bethe lattice under an applied magnetic field studied by means of exact recursion equations method. All the thermodynamical quantities of interest are obtained in terms of recursion equations.

The ground-state phase diagram of the model was constructed as shown in Figure 2. In this phase diagram, we have found eight stable phases and along the $\frac{D}{q|J|}$-axis, two particular hybrid phases are located at two multicritical points, namely A_6 and A_7. This ground-state phase diagram is used as a guide in obtaining the different finite-temperature phase diagrams. We also investigated in the presence and the absence of longitudinal magnetic field h, the thermal variations of sublattice magnetizations, the corresponding response functions, the internal energy and the free energy as seen in Figures (3)−(8). From these figures, the order parameters showed in most cases, the usual decay with thermal fluctuations. By using the thermal behaviors of the considered order parameters, the analysis of the corresponding response functions, the internal energy and the free energy, the nature of the different phase transitions encountered is identified. This enables us to present and discuss in detail the different finite-temperature phase diagrams in the case of equal crystal field interactions as shown in Figure (9)−(11). We have found that the model presents very rich critical behaviors, which include first-order and second-order transitions as well as tricritical points in the physical parameters' space. We have also found that the model displays the compensation phenomenon where the compensation points were identified for appropriate values of the crystal field interactions.

Finally, we should mention that the different results achieved here bear some topological resemblances with those reported in [20, 21, 25].

Acknowledgements

The authors thank Prof C. Ekiz for useful comments on the manuscript.

Disclosure statement

No potential conflict of interest was reported by the authors.

References

[1] Thompson CJ. Mathematical statistical mechanics. Princeton (NJ): Princeton University Press; 1992.
[2] Strečka J, Jaščin M. A brief account of the Ising and Ising-like models: mean-field effective-field and exact results. Acta Phys Slovaca. 2015;65:235–367.
[3] Lacková S, Jaščur M, Horiguchi T. Exact results of a mixed spin-1/2 and spin -1 transverse Ising model with two- and four-spin interactions and crystal field on the honeycomb lattice. Phys A. 2004;339:416–436.
[4] Strečka J. Exact results of a mixed spin-1/2 and spin-S Ising model on a bathroom tile (4–8) lattice: effect of uniaxial single-ion anisotropy. Phys A. 2006;360:379–390.
[5] Jaščur M, Strečka J. Reentrant transition of a mixed-spin Ising model on the diced lattice. Condens Matter Phys. 2005;8:869–880.
[6] White R.M. Opportunities in magnetic materials. Science. 1985;229:11–15.
[7] Wood R. Understanding magnetism. Blue Ridge Summit (PA): Tab Books Inc.; 1988.
[8] Köster E. Trends in magnetic recording media. J Magn Magn Mater. 1988;120:1–10.
[9] Lueck LB, Gilson RG. Challenges and opportunities: the magnetic media industry in the 1990s. J Magn Magn Mater. 1999;88:227–235.
[10] Itoh K, Kinoshita M. Molecular magnetism: new magnetic materials. Tokyo: Kodansha; 2000.
[11] Linert W, Verdaguer M, editors,. Molecular magnets: recent highlights. Berlin: Springer; 2003.
[12] Gatteschi D. Molecular magnetism: a basics for new materials. Adv Matter. 1994;6:635–645.
[13] Miller JS, Epstein AJ. Designer magnets. Chem Eng News. 1995;73:30–41.
[14] Kahn O. Molecular magnetism. New York (NY): VCH; 1993.
[15] Bobák A. The effect of anisotropies on the magnetic properties of a mixed spin-1 and spin-3/2 Ising ferrimagnetic system. Phys A. 1998;258:140–156.
[16] Benyoussef A, El Kenz A, Kaneyoshi T. Tricritical behaviour in diluted mixed spin-1 and spin-1/2 on square lattice. J Magn Magn Mater. 1994;131:179–182.
[17] Bobák A, Jurcišin M. A discussion of critical behaviour in a mixed -spin Ising model. Phys A. 1997;240:647–656.
[18] de Oliveira DC, Silva AAP, de Albuquerque DF, et . Critical behavior of an Ising metamagnetic in uniform and random fields. Phys A. 2007;386:205–211.
[19] Kaneyoshi T. Tricritical behavior of a mixed spin-1/2 and spin-2 Ising system. Phys. A. 1994;205:677–686.
[20] Canpolat Y, Torgürsül A, Polat H. The magnetic properties of spin-1/2 and spin-1 Ising models in an applied magnetic field by introducing the effective-field approximation. Phys Scr. 2007;76:597–605.
[21] Deviren B, Bati M, Keskin M. The effective-field study of a mixed spin-1 and spin-5/2 ferrimagnetic system. Phys Scr. 2009;79:065006.
[22] da Cruz Filho JS, Godoy M, Arruda AS. Phase diagram of the mixed spin-2 and spin-5/2 Ising system with two different single-ion anisotropies. Phys A. 2013;392:6247–6254.
[23] Miao H, Wei G, Geng J. Phase transitions and multicritical points in the mixed spin-3/2 and spin-2 Ising model with different single-ion anisotropies. J Magn Magn Mater. 2009;321:4139–4144.
[24] Mohamad HK, Domashevskaya EP, Klinskikh AF. Spin compensation temperatures in the mean-field approximation of a mixed spin-2 and spin-5/2 Ising ferrimagnetic system. Phys A. 2009;388:4713–4718.
[25] Mohamad HK. Magnetic and thermodynamic properties of a mixed spin-1 and spin-7/2 Blume–Capel Ising ferrimagnetic system. Int J Adv Res. 2014;9:442–453.
[26] Kaneyoshi T, Chen JC. Mean-field analysis of a ferrimagnetic mixed spin system model. J Magn Magn Mater. 1991;98:201–204.
[27] Quadros SGA, Salinas SR. Renormalization group calculation for a mixed-spin Ising model. Phys A. 1994;206:479–496.
[28] El Bouziani M, Gaye A, Jellal A. Position space renormalization group study of the spin-1 random semi-infinite Blume-Capel model. Phys A. 2013;392:689–701.
[29] Buendia GM, Liendo JA. Monte Carlo simulation of a mixed spin-1/2 and spin-3/2 Ising ferrimagnetic system. J Phys Condens Matter. 1997;9:5439–5448.
[30] Godoy M, Figueiredo W. Nonequilibrium antiferromagnetic mixed-spin Ising model. Phys Rev E. 2002;66:036131–036136.
[31] Cambui DS, Arruda AS, Godoy M. Monte Carlo simulations of disordered binary Ising model. Int J Mod Phys C. 2012;23:1240015.
[32] Feraoun A, Zaim A, Kerouad M. Monte Carlo study of a mixed spin (1, 3/2) ferrimagnetic nanowire with core/shell morphology. Phys B. 2014;445:74–80.
[33] Zukovic M, Bobák A. Critical and compensation phenomena in a mixed-spin ternary alloy: a Monte Carlo study. J Magn Magn Mater. 2010;322:2868–2873.
[34] Yessoufou RA, Bekhechi S, Hontinfinde F. Numerical study of the mixed spin-1 and spin-5/2 BEG model of the Bethe lattice. Eur Phys J B. 2011;81:137–146.
[35] Kple J, Yessoufou RA, Hontinfinde F. The mixed spin-1 and spin-5/2 BEG model in a staggered magnetic field. Afr Rev Phys. 2012;7:319–335.

[36] Albayrak E, Yigit A. Critical properties of mixed spin-1 and spin-5/2 with equal and unequal crystal fields. Chin Phys B. 2012;21:020511−020518.
[37] Albayrak E. Mixed spin-1 and spin-3/2 Blume-Capel Ising ferrimagnetic system on the Bethe lattice. Int J Mod Phys B. 2008;17:1087−1100.
[38] Albayrak E., Yigit A. Mixed spin-3/2 and spin-5/2 Ising system on the Bethe lattice. Phys Lett A. 2006;353:121−129.
[39] Karimou M, Yessoufou R, Hontinfinde F. Critical behaviors and phase diagrams of the mixed spin-1 and spin-7/2 Blume-Capel Ising model on the Bethe lattice. Int J Mod Phys B. 2015;29:1550194-1−1550194-19.
[40] Ekiz C. The possibility of two compensation points in a ferrimagnetic mixed spin-1 and spin-3/2 Ising system using the Bethe lattice approach. J Magn Magn Mater. 2006;307:139−147.
[41] Metropolis NC, Rosenbluth AW, Rosenbluth MN, Teller E. Equation of state calculations by fast computing machines. J Chem Phys. 1953;21:1087−1092.
[42] Ekiz C, Strečka J, Jaščur M. Mixed spin-1/2 and spin-1 Ising model with uniaxial and biaxial single-ion anisotropy on the Bethe lattice. Cent Eur J Phys. 2009;7:509−520.